

Linear Combination of Saved Checkpoints Makes Consistency and Diffusion Models Better

Enshu Liu^{*1,2}, Junyi Zhu^{*3}, Zinan Lin^{†‡4}, Xuefei Ning^{†‡1},
Matthew B. Blaschko³, Sergey Yekhanin⁴, Shengen Yan²,
Guohao Dai^{2,5}, Huazhong Yang¹, and Yu Wang^{‡1}

¹ Tsinghua University

² Infinigence-AI

³ KU Leuven

⁴ Microsoft Research

⁵ Shanghai Jiao Tong University

Abstract. Diffusion Models (DM) and Consistency Models (CM) are two types of popular generative models with good generation quality on various tasks. When training DM and CM, intermediate weight checkpoints are not fully utilized and only the last converged checkpoint is used. In this work, we find that high-quality model weights often lie in a basin which cannot be reached by SGD but can be obtained by proper checkpoint averaging. Based on these observations, we propose LCSC, a simple but effective and efficient method to enhance the performance of DM and CM, by combining checkpoints along the training trajectory with coefficients deduced from evolutionary search. We demonstrate the value of LCSC through two use cases: **(a) Reducing training cost.** With LCSC, we only need to train DM/CM with fewer number of iterations and/or lower batch sizes to obtain comparable sample quality with the fully trained model. For example, LCSC achieves considerable training speedups for CM (23× on CIFAR-10 and 15× on ImageNet-64). **(b) Enhancing pre-trained models.** Assuming full training is already done, LCSC can further improve the generation quality or speed of the final converged models. For example, LCSC achieves better performance using 1 number of function evaluation (NFE) than the base model with 2 NFE on consistency distillation, and decreases the NFE of DM from 15 to 9 while maintaining the generation quality on CIFAR-10. Our code is available at <https://github.com/imagination-research/LCSC>.

Keywords: Consistency Model · Diffusion Model · Weight Averaging · Evolutionary Search

1 Introduction

Diffusion Models (DMs) [8, 36, 40] are a newly emerged paradigm of generative modeling and have gained widespread attention rapidly in the last several

* Equal Contribution

† Co-advise

‡ Corresponding Authors: Yu Wang (yu-wang@mail.tsinghua.edu.cn), Xuefei Ning (foxdoraame@gmail.com) and Zinan Lin (zinanlin@microsoft.com).

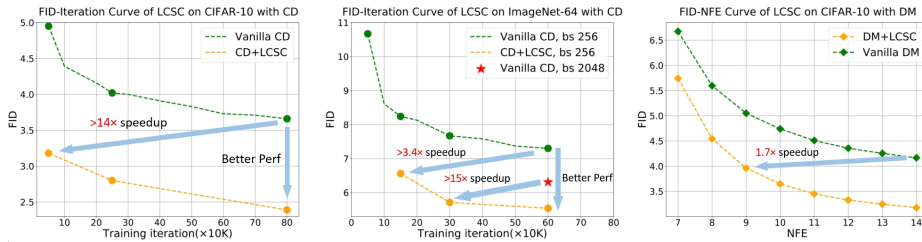


Fig. 1: Comparison of LCSC and vanilla training. LCSC achieves more than $14\times$ training speed up on CIFAR-10 with Consistency Distillation (CD) and more than $15\times$ training speed up compared to official released model on ImageNet-64 with CD. LCSC can also enhance the final converged model significantly and achieves $1.7\times$ inference speedup for DM.

years. DM achieves surprising performance in various tasks like image generation [4, 8, 33], video generation [2, 9] and 3D generation [20, 31]. However, DM requires an iterative denoising process in the generation process, which could be slow. Consistency Models (CMs) [39] are proposed to handle this dilemma. CM provides a better generation quality under one or few-step generation scenarios and is applied in many practical cases [25, 26, 43].

In this paper, we investigate the training process of DM and CM. We find that checkpoints—the model weights periodically saved during the training process—have under-exploited potential in boosting the performance of DM and CM. Specifically, there are numerous high-quality basins located near any given point along the optimization trajectory in the metric landscape. These high-quality basins *cannot* be reliably reached through Stochastic Gradient Descent (SGD), including its advanced variants like Adam [16]. However, we find that an appropriate linear combination of different checkpoints can locate these basins.

Inspired by the observation, we propose to find a Linear Combination of Saved Checkpoints (LCSC) that optimizes the model performance. Specifically, for a set of checkpoints saved until any point of the training process, LCSC searches for the optimal linear combination weights that optimize certain metrics (e.g., FID [7]) using an evolutionary algorithm. Note that the widely used Exponential Moving Average (EMA) [42] in DM and CM can be viewed as a special case of LCSC whose combination coefficients are determined heuristically and we will show in our experiments that EMA coefficients are sub-optimal. LCSC optimizes only in a low-dimension space and needs no back-propagation, thus could be faster than training. LCSC can optimize objectives or metrics whose gradients are hard to compute (e.g., FID), under which gradient-based optimization is not applicable. From a broader perspective, LCSC is a general method and may be used in other tasks and other neural networks.

We argue that LCSC is beneficial in all steps in the DM/CM production stage. For example, LCSC can be used to:

Reduce training cost. The training process of DM and CM is very costly. For example, training an EDM model [15] on CIFAR-10 costs about 2 days with 8 V100 GPUs, and training a CM model [39] costs about one week with 8 A100 GPUs. For datasets with higher resolution, the training cost is even

larger. On ImageNet-64, SOTA DMs and CMs [4, 15, 39] are trained with a batch size of several thousand on 32 or 64 A100 GPUs for about one week, consuming very huge computational resources. *With LCSC applied at the end, we can train CM/DM with many fewer iterations or smaller batch sizes and reach similar generation quality with the fully trained model, thereby reducing the computational cost of training.*

Enhance pre-trained models. Assuming the full training is already done, LCSC can still be applied to get a model that is *better than any model in the training process*. For model developers with saved checkpoints, LCSC can be directly applied. For users who can only access the final released checkpoint, they can fine-tune the model for a few more iterations and apply LCSC on these checkpoints. As DM/CM provides a flexible trade-off between generation quality and the number of generation steps, *the enhanced model from LCSC could lead to either better generation quality or faster generation.*

In conclusion, the contributions of this paper are as follows:

In Sec. 3, we analyze the metric landscape of DM and CM. We demonstrate that there are basins with better generation quality that cannot be reached through traditional SGD but can be achieved by linear combinations of checkpoints. We further demonstrate the sub-optimality of the commonly used EMA, illustrating the importance of exploring better ways of weight combination.

In Sec. 4, we propose our simple but effective method LCSC to address the problem. LCSC employs evolutionary search to optimize linear combination coefficients of previous checkpoints. LCSC has two use cases: **(1)** reducing training cost and **(2)** enhancing pre-trained models. LCSC needs no back-propagation and has the potential to be applied to other tasks and models.

In Sec. 5, we validate the effectiveness of LCSC on DM and CM for the two use cases. LCSC accelerates the training process of Consistency Distillation (CD) and Consistency Training (CT) by $23\times$ and $7\times$ on CIFAR-10, and $15\times$ and $10.4\times$ on ImageNet-64. Additionally, we apply LCSC to enhance the pre-trained models. For DM, LCSC by combining pre-trained checkpoints decreases the NFE from 15 to 9 while keeping the sample quality. For CM, LCSC achieves better performance with 1 NFE compared to the vanilla final model with 2 NFE. With the same NFE, models from LCSC have much better sample quality.

In Sec. 6, we present and discuss the searched patterns of combination coefficients to inspire further research on weights combination. Then we discuss the reasons why LCSC works due to the unique properties of DM and CM.

2 Background and Related Work

2.1 Diffusion Probabilistic Model

Let us denote the data distribution by p_{data} and consider a diffusion process that perturbs p_{data} with a stochastic differential equation (SDE) [40]:

$$d\mathbf{x}_t = \boldsymbol{\mu}(\mathbf{x}_t, t)dt + \sigma(t)d\mathbf{w}_t, \quad (1)$$

where $\boldsymbol{\mu}(\cdot, \cdot)$ and $\sigma(\cdot)$ represent the drift and diffusion coefficients, respectively, \mathbf{w}_t denotes the standard Brownian motion, and $t \in [0, T]$ indicates the time step.

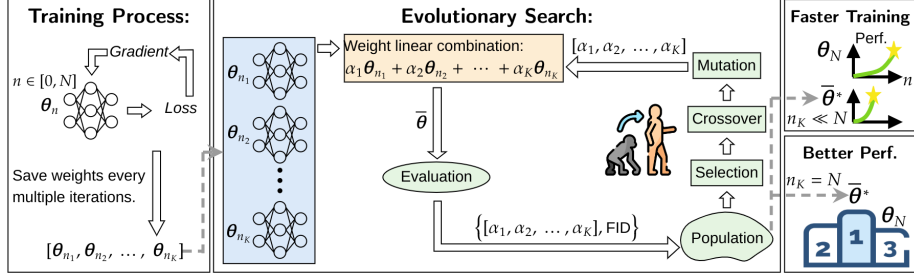


Fig. 2: A schematic diagram of LCSC. Given a set of checkpoints from training, LCSC use evolutionary search to find the optimal linear combination weights. LCSC can be applied on checkpoints from a training process with fewer training iterations or batch sizes and still gets similar performance (abbreviated as “Perf.”), thus reducing training cost and enabling faster training. LCSC can also enhance the final model in terms of generation quality or speed.

$t = 0$ stands for the real data distribution. $\mu(\cdot, \cdot)$ and $\sigma(\cdot)$ are designed to make sure $p_T(\mathbf{x})$ becomes pure Gaussian noise.

Diffusion models (DM) [4, 8, 15, 28, 36, 37, 40] undertake the reverse operation by initiating with \mathbf{x}_T sampled from pure Gaussian noise and progressively denoising it to reconstruct the image \mathbf{x}_0 . Importantly, SDE has its corresponding “probability flow” Ordinary Differential Equation (PF ODE) [37, 40], which delineates a deterministic pathway that yields the same distribution $p_t(\mathbf{x})$ for $\forall t$, thereby offering a more efficient sampling mechanism:

$$d\mathbf{x}_t = \left[\boldsymbol{\mu}(\mathbf{x}_t, t) - \frac{1}{2}\sigma(t)^2\nabla\log p_t(\mathbf{x}) \right] dt, \quad (2)$$

where $\nabla\log p_t(\mathbf{x})$ is referred to as the *score function* of $p_t(\mathbf{x})$ [10]. Various ODE solvers have been introduced to further expedite the sampling process utilizing Eq. (2) or minimizing the truncation error [14, 15, 23, 24].

A pivotal insight within diffusion models is the realization that $\nabla\log p_t(\mathbf{x})$ can be approximated by a neural network $\mathbf{s}_\theta(\mathbf{x}_t, t)$, which can be trained using the following objective:

$$\mathbb{E}_{t\sim\mathcal{U}(0,T)}\mathbb{E}_{\mathbf{y}\sim p_{\text{data}}}\mathbb{E}_{\mathbf{x}_t\sim\mathcal{N}(\mathbf{y},\sigma(t)^2\mathbf{I})}\lambda(t)\|\mathbf{s}_\theta(\mathbf{x}_t, t) - \nabla_{\mathbf{x}_t}\log p(\mathbf{x}_t|\mathbf{y})\|, \quad (3)$$

where $\lambda(t)$ represents the loss weighting and \mathbf{y} denotes a training image.

2.2 Consistency Models

Drawing inspiration from DM theory, consistency models (CM) have been proposed to enable single-step generation [38, 39]. Whereas DM incrementally denoises an image, e.g., via the PF ODE, CM denoted by f_θ is designed to map any point \mathbf{x}_t at any given time t along a PF ODE trajectory directly to the trajectory’s initial point \mathbf{x}_t in a single step.

CMs are usually trained through discretized time steps, so we consider segmenting the time span from $[\epsilon, T]$ into $K - 1$ sub-intervals, with ϵ being a small value approximating zero. Training of CM can follow one of two primary methodologies: consistency distillation (CD) or direct consistency training (CT). In the

case of CD, the model f_{θ} leverages knowledge distilled from a pre-trained DM ϕ . The distillation loss can be formulated as follows:

$$\mathbb{E}_{k \sim \mathcal{U}[1, K-1]} \mathbb{E}_{\mathbf{y} \sim p_{data}} \mathbb{E}_{\mathbf{x}_{t_{k+1}} \sim \mathcal{N}(\mathbf{y}, t_{k+1}^2 \mathbf{I})} \lambda(t_k) d(f_{\theta}(\mathbf{x}_{t_{k+1}}, t_{k+1}), f_{\theta^-}(\hat{\mathbf{x}}_{t_k}^{\phi}, t_k)), \quad (4)$$

where f_{θ^-} refers to the target model and θ^- is computed through EMA (see Eq. (6)) of the historical weights of θ , $\hat{\mathbf{x}}_{t_k}^{\phi}$ is estimated by the pre-trained diffusion model ϕ through one-step denoising based on $\mathbf{x}_{t_{k+1}}$, and d is a metric implemented by either the ℓ_2 distance or LPIPS [49].

Alternatively, in the CT case, the models f_{θ} are developed independently, without relying on any pre-trained DM:

$$\mathbb{E}_{k \sim \mathcal{U}[1, K-1]} \mathbb{E}_{\mathbf{y} \sim p_{data}} \mathbb{E}_{\mathbf{z} \sim \mathcal{N}(\mathbf{0}, \mathbf{I})} \lambda(t_k) d(f_{\theta}(\mathbf{y} + t_{k+1} \mathbf{z}, t_{k+1}), f_{\theta^-}(\mathbf{y} + t_k \mathbf{z}, t_k)), \quad (5)$$

where the target model f_{θ^-} is set to be the same as the model f_{θ} in the latest improved version of the consistency training [38], i.e. $\theta^- = \theta$.

2.3 Weight Averaging

The integration of a running average of the weights by stochastic gradient descent (SGD) was initially explored within the realm of convex optimization [30, 34]. This concept was later applied to the training of neural networks [42]. Izmailov et al. [12] suggest that averaging multiple weights over the course of training can yield better generalization than SGD. Wortsman et al. [45] demonstrate the potential of averaging weights that have been fine-tuned with various hyper-parameter configurations. The Exponential Moving Average (EMA) employs a specific form that uses the exponential rate γ as a smoothing factor:

$$\tilde{\theta}_n = \gamma \tilde{\theta}_{n-1} + (1 - \gamma) \theta_n, \quad (6)$$

where $n = 1, \dots, N$ denotes the number of training iterations, $\tilde{\theta}$ represents the EMA model, and is initialized with $\tilde{\theta}_0 = \theta_0$.

Practitioners often opt for advanced optimizers such as Adam [16] for different tasks and network architectures, which might reduce the need for employing a running average. However, the use of EMA has been noted to significantly enhance the quality of generation in early DM studies [4, 8, 28, 37, 40]. This empirical strategy has been adopted in most, if not all, subsequent research endeavors. Consequently, CM have also incorporated this technique, discovering EMA models that perform substantially better.

Recently, several works of more advanced weight averaging strategies have been proposed for Large Language Models (LLMs). Most of them focus on merging models fine-tuned for different downstream tasks to create a new model with multiple capabilities [11, 13, 46, 48]. Different from these approaches, our work aims to accelerate the model convergence and achieve better performance in a standalone training process. Moreover, the methodology we employ for determining averaging coefficients is novel, thereby distinguishing our method from these related works. Further details can be found in Sec. 3 and Sec. 4.

2.4 Search-based Methods for Diffusion Models

Search algorithms are widely used across various domains like Neural Architecture Search (NAS) [29, 32], where they are employed to identify specific targets. Recently, many works studies have set discrete optimization dimensions for DMs and utilized search methods to unearth optimal solutions. For example, Liu et al. [21], Li et al. [19] and Yang et al. [47] use search methods to find the best model schedule for DMs. Liu et al. [22] apply search methods to find appropriate strategies for diffusion solvers. However, these works do not involve modification to model weights during search and are only applicable to DMs.

3 Motivation

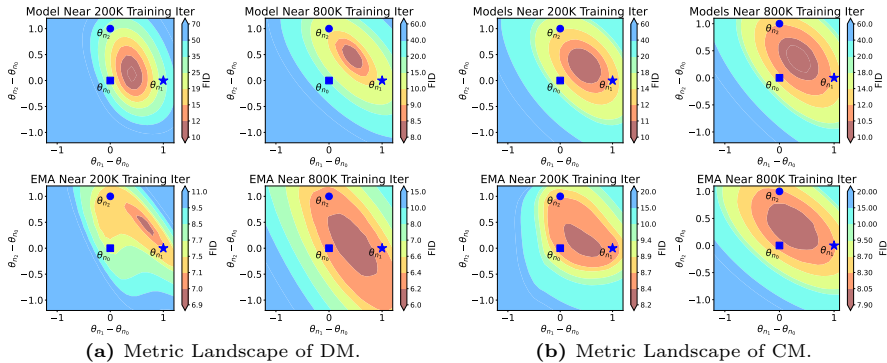


Fig. 3: The metric landscape of the diffusion model. Selected checkpoints θ_{n_0} , θ_{n_1} , and θ_{n_2} are aligned sequentially along the training trajectory, with $n_0 < n_1 < n_2$ denoting the progression in the number of training iterations. The origin point $(0, 0)$ corresponds to the checkpoint θ_{n_1} , while the X and Y axes quantify the differences between $\theta_{n_1} - \theta_{n_0}$ and $\theta_{n_2} - \theta_{n_0}$, respectively. A weight located at coordinate (x, y) is formulated as $\theta_{(x,y)} = \theta_{n_0} + x(\theta_{n_1} - \theta_{n_0}) + y(\theta_{n_2} - \theta_{n_0})$. Additional visualizations are provided in App. A.

One notable challenge associated with DMs and CMs is their difficulty in training. We observe that the objectives for DMs and CMs tend to produce substantial variance in gradient estimations, leading to fluctuations in the quality of generation by the resulting models. For DMs (refer to Eq. (3)), even if the networks s_{θ} are finely tuned to perfectly mirror the score function $\nabla \log p_t(\mathbf{x})$ for any given \mathbf{x}_t , the loss as defined does not reduce to zero. As a result, the batched gradient estimation for this objective exhibits high variance. For CMs (refer to Eqs. (4) and (5)), at any given time t , the network f_{θ} is solely optimized to align with the target model f_{θ^-} from the previous time step, $t - 1$. This implies that any loss of image information in the early time steps could result in inaccurate gradient estimation in subsequent time steps.

To explore the training challenges of DMs and CMs, we visualize the landscape of generation quality in a 2-dimension (2D) plane. Specifically, we select 3 checkpoints of the weights $\theta_{n_0}, \theta_{n_1}, \theta_{n_2}$ from the same training trajectory. We

then sweep across the 2D space spanned by these three points to assess the FID scores. The results are shown in the first row of Fig. 3. As we can see, there exist model weights with much higher generation quality than any of $\{\theta_{n_0}, \theta_{n_1}, \theta_{n_2}\}$ in the sub-space spanned by those three checkpoints for both DM and CM. Additionally, results at different training iterations indicate that this pattern of landscape remains stable in different training stages. These insights imply that there exists a substantial opportunity to enhance the model’s performance at any training phase through the linear combination of existing weight checkpoints.

EMA [42] is simple yet widely used technique in the training of DMs and CMs. It operates by exponentially averaging the weights of all previous checkpoints (see Eq. (6)), which stabilizes the training process of DMs and CMs to a certain extent. Nonetheless, EMA represents an empirical method of averaging, suggesting potential areas for enhancement. To investigate this hypothesis, we conducted an experiment where the three checkpoints from previous tests were substituted with three EMA weights, followed by a comprehensive re-sweep of all coordinates. The results are demonstrated in the second row of Fig. 3. Notably, it is observed that a linear combination of the three EMA weights could achieve superior performance compared to each individual weight. It is important to highlight that the linear combination of three EMA weights at various training iterations cannot be replicated by simply adjusting EMA rates. Consequently, this suggests that EMA may indeed be a sub-optimal solution, indicating possibilities for further improvement in this area.

Based on the above insights and the observation, we propose LCSC, standing for Linear Combination of Saved Checkpoints, to enhance the training process. Since the basin in Fig. 3 extends beyond the convex hull of the model weights, we further expand the scope of the combination coefficients to encompass any real values and introduce an optimization method to search for the optimal linear combination of the weights.

4 Method

We discuss LCSC in this section. The search problem is defined in Sec. 4.1. In Sec. 4.2, we elaborate on our algorithm. Finally, we list several typical use cases of our method in Sec. 4.3.

4.1 Problem Definition

Let $\{1, 2, \dots, N\}$ denote the set of training iterations. Suppose $\{n_1, n_2, \dots, n_K\}$ is a subsequence selected from $\{1, 2, \dots, N\}$. Define Θ as the set of checkpoints saved at these specific training iterations: $\Theta = \{\theta_{n_1}, \theta_{n_2}, \theta_{n_3}, \dots, \theta_{n_K}\}$. Given Θ , we aim to find a group of coefficients $\alpha = \{a_1, a_2, a_3, \dots, a_K\}$. These coefficients are intended to linearly combine all the checkpoints in such a way that the resulting model achieves the optimal performance:

$$\arg \min_{a_1, a_2, a_3, \dots, a_K \in \mathbb{R}} \mathcal{F}(a_1 \theta_{n_1} + a_2 \theta_{n_2} + a_3 \theta_{n_3}, \dots, a_K \theta_{n_K}); \quad \text{s.t.} \quad \sum_{i=1}^K a_i = 1, \quad (7)$$

where $\mathcal{F}(\boldsymbol{\theta})$ denotes an evaluation function that measures the generation quality of $\boldsymbol{\theta}$ regarding a specific metric, indicating higher quality with a smaller value. The constraint $\sum_{i=1}^K a_i = 1$ reduces the dimension of our search space by 1. However, we find it enables a more effective exploration for the search algorithm.

4.2 Evolutionary Search

When the number of combined checkpoints K is large (e.g., ranges approximately from 200 to 500 in our experiments), the grid search method used in Sec. 3 becomes inefficient. Consequently, we propose to use evolutionary search [19, 21, 22, 32, 47] to solve the problem.

Our detailed algorithm can be found in Alg. 1. Given a set of checkpoints Θ , we can apply this algorithm at any training iteration n along the training trajectory. We initialize the population using EMA coefficients corresponding to several different rates. Then we conduct an evolutionary search which views a group of coefficients as an individual. In each search iteration, only the top-performing individuals are selected as parents to reproduce the next generation through crossover and mutation. Specifically, during crossover, we randomly mix the coefficients of the two parents or select one of them. For mutation, we introduce random Gaussian noise to each coefficient. This stochastic element ensures that positive adaptations in the coefficients are conserved and advanced to the subsequent generation, whereas detrimental modifications are discarded. Finally, we normalize the new coefficients to adhere to the regularization condition in Eq. (7). We repeat this reproduction process for a predetermined number of times within each search iteration and update the whole population with all newly generated individuals. Upon the completion of the search process, we choose the best individual as the output of our search algorithm.

Given the absence of neural back-propagation in the search process, LCSC can be viewed as a gradient-free optimization method, akin to methods discussed in [27, 41]. This characteristic renders LCSC highly efficient in terms of computation, offering significant savings in GPU memory usage (applicable to both DM and CM) and computational time (specifically for CM, given that the inference process for DM is notably resource-intensive). Furthermore, LCSC possesses the unique advantage of optimizing models directly towards non-derivable metrics where gradient-based methods falter. It is also important to underscore that the applicability of LCSC extends beyond CM and DMs to various other tasks and different models.

4.3 Use Cases

In this section, we delve into the use cases of our method. **(1)** Our method can be employed during the initial phases of the training process or in scenarios where the training is conducted with a smaller batch size. This application aims to expedite the training process; **(2)** At the final stage of training, when the model has essentially converged, our method can be utilized to further enhance the model’s performance. This involves refining the output quality of the already converged model and potentially reducing NFE.

Algorithm 1 Evolutionary Search for Combination Coefficients Optimization**Require:**

$\Theta = \{\theta_{n_1}, \theta_{n_2}, \theta_{n_3}, \dots, \theta_{n_K}\}$: the set of saved checkpoints until training iter T
 \mathcal{F} : the metric evaluator.

Symbols:

P : The whole Population of model schedule.
 CP : The Candidate Parents set of each loop, from which a parent model schedule is selected.
 NG : The Next Generation newly mutated from the parent schedule in each loop.
 α : A group of combination coefficients denoted as $\alpha = \{a_0, a_1, \dots, a_K\}$
 $\alpha \cdot \Theta$: Equal to $\sum_{i=1}^K \alpha_i \theta_{n_i}$

Hyperparameters:

Epoch: Number of loops for the entire search process.
 M_{CP} : Maximum size of the candidate parents set CP .
Iter: Maximum number of mutations in each loop.

Search Process:

```

1:  $P \leftarrow \emptyset$ 
2: Initialize a group of coefficients  $\alpha_{init}$  with EMA weights
3:  $P \leftarrow P \cup \{(\alpha_{init}, \mathcal{F}(\alpha_{init} \cdot \Theta))\}$ 
4: for  $t = 1, \dots, \text{Iter}$  do
5:    $NG \leftarrow \emptyset$ 
6:   for  $i = 1, \dots, \text{Epoch}$  do
7:      $CP \leftarrow \{\alpha_i | \mathcal{F}(\alpha_i \cdot \Theta) \text{ ranks within the top } \min(M_{CP}, |P|) \text{ in } P\}$ 
8:      $\alpha_f, \alpha_m \xleftarrow{\text{Random Sample}} CP$ 
9:      $\alpha_{new} \leftarrow \text{Mutate}(\text{Crossover}(\alpha_f, \alpha_m))$ 
10:     $\alpha_{new} \leftarrow \alpha_{new} / \text{sum}(\alpha_{new})$ 
11:     $NG \leftarrow NG \cup \{(\alpha_{new}, \mathcal{F}(\alpha_{new} \cdot \Theta))\}$ 
12:   end for
13:    $P \leftarrow P \cup NG$ 
14: end for
15:  $\alpha^* \leftarrow \arg \min_{\alpha \in P} \mathcal{F}(\alpha \cdot \Theta)$ 
16: return  $\alpha^* \cdot \Theta$ 

```

Decrease Training Cost. The consumption of training resources is directly influenced by both the number of iterations and the batch size. Through our investigation, we have discerned that the training process for Diffusion Models (DM) and Consistency Models (CM) can be categorized into two distinct phases, as illustrated in Fig. 4. The initial phase is relatively brief, during which DM and CM rapidly acquire the capability to generate visually satisfactory images. In contrast, the second phase is characterized by a slower optimization of models, focusing on the enhancement of sample quality. Implementing LCSC at the onset of this second phase can facilitate an efficient identification of high-quality basins, potentially yielding performance that is on par with, or even surpasses, that of the final converged model. This strategy effectively reduces the total number of training iterations required. Regarding *batch size*, SOTA DMs and CMs necessitate training with large batch sizes [4, 15, 39], which places a sub-

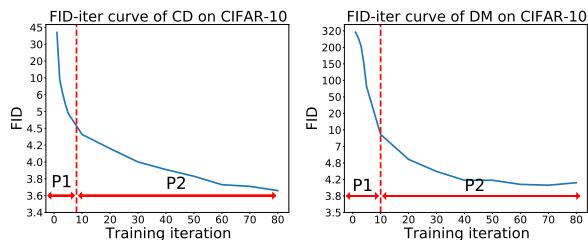


Fig. 4: Training curves on CIFAR-10 with CM and DM. P1, P2 represent the first phase and the second phase.

stantial demand on hardware and computational resources. Decreasing the batch size often leads to worse convergence performance. LCSC can be used for low batch size training and achieve equivalent performance to models trained with full batch size.

Enhance Converged Models. LCSC can also be applied to the checkpoints saved during the final stage of training to enhance the performance of converged models. Furthermore, for users who have access to released pre-trained models, we suggest fine-tuning the model for a few iterations and saving the intermediate checkpoints. Then LCSC can be used to enhance the released model.

5 Experiments

In this section we present our experiments to validate the effectiveness of LCSC. In Sec. 5.1, we introduce the experimental settings. Then we demonstrate our results on CM and DM for the two use cases in Sec. 5.2. We finally ablate several important hyper-parameters in our workflow in Sec. 5.3.

5.1 Experimental Setup

For DM, we follow DDIM [37] for the evaluation on CIFAR10 [17] and iD-DPM [28] for the evaluation on ImageNet-64 [3]. To improve the inference efficiency, we adopt DPM-Solver [24]. For CM [39], we evaluate LCSC with both CD and CT on CIFAR-10 and ImageNet-64. We train models with our own implementation. We follow all the settings reported by the official paper except ImageNet-64, on which we decrease the batch size to 256 on CM and 512 on DM due to the limited resources. We applied LCSC at different training stages. Specifically, for any selected iteration, we utilize checkpoints from every pre-determined interval of iterations within a defined window size. Then we run a search process to find the optimal combination coefficients.

Evaluation. We choose the most commonly used metric, FID [7], as the search objective. To evaluate the combination coefficients during the evolutionary search, we sample 5K images on ImageNet-64 with DM and 10K in other settings, using a fixed group of initial noise. For the final model evaluation, we generate 50K samples using another group of initial noises. To demonstrate that LCSC is not overfitted to FID but achieves overall improvement, we report on FID, IS [35], precision [18], and recall [18]. In App. B.5, we further report FID@Clip to show that LCSC also brings improvements in other feature spaces.

Baselines. Since EMA is the default setting in almost all works of DM and CM, we report the performance of the EMA weights using the rate reported by official papers [28, 37, 39] as our main baselines. For CM models on ImageNet-64,

we additionally download the official models trained with full batch size and test their performance for a complete comparison. We further conduct a grid search of EMA rate for the final model as a stronger baseline, denoted as EMA*, to prove the sub-optimality of EMA and that LCSC is a more effective method. More experimental details are provided in App. B.

5.2 Results

Our results for CM are shown in Tab. 1 and Tab. 2, while for DM, the results are presented in Tab. 3. By conducting LCSC, we consistently find models that outperform the current EMA model across all settings. Although LCSC searches according to FID, consistent improvements are observed across different metrics. Notably, improvement is evident even at the early stages of training, e.g., 50K iterations, when the model is not yet fully trained. Below, we discuss our results under two use cases: decreasing training costs and enhancing the final converged model. Generated images are visualized in App. E.

Results on Decreasing the Training Cost We conduct a series of experiments using CD and CT to validate that LCSC can significantly reduce training costs. Our reported speedup results have been adjusted to include the search cost on both CPU and GPU, with detailed information available in App. B.2.

LCSC can be applied at an early training stage to decrease the number of training iterations. As illustrated in Tab. 1, for CIFAR-10, applying LCSC to the model with only 50K training iterations achieves a better FID than the final model trained with 800K iterations (3.18 vs. 3.65) while accelerating the training by approximately $14\times$ for CD. For CT, we only achieve a converged FID of 9.87 with vanilla training and fail to fully reproduce the result of FID=8.70 reported by Song et al. [39]. However, by applying our method at 400K training iterations, we can still surpass the reported FID by Song et al. [39] with 800K training iterations, achieving around a $1.9\times$ speedup. On ImageNet-64, we decrease the batch size from 2048 to 256 due to limited resources. For CD, LCSC achieves better performance (6.56, 5.71 vs. 7.30 in FID) than the final converged model with only a quarter or half of the training iterations (150K, 300K vs. 600K). For CT, LCSC also significantly reduces the final converged FID (12.05 vs. 15.56) with fewer training iterations (600K vs. 800K).

LCSC can also contribute to reducing the training batch size. On CIFAR-10, we train another model with a lower batch size to validate LCSC’s performance under these conditions. As illustrated in Tab. 1, LCSC with a batch size of 128 outperforms the final converged model with a batch size of 512 for both CD and CT (3.34 vs. 3.65 with CD and 8.33 vs. 8.70, 9.87 with CT), achieving overall speedups of $23\times$ and $7\times$, respectively. On ImageNet-64, we test the official models of Song et al. [39], which were trained with a 2048 batch size for both CD and CT. With the assistance of LCSC, models trained with a 256 batch size consistently outperform the official models (5.71, 5.54 vs. 6.31 with CD and 12.05 vs. 13.07 with CT), achieving overall acceleration ratios of $15\times$ and $10.4\times$.

Results on Enhancing Pre-trained Models Our experiments on both DM and CM show that LCSC can significantly boost the performance of final converged models and reduce the required sampling steps.

Table 1: Generation quality of consistency models on CIFAR-10. The training speedup is compared against the standard training with 800K iterations and 512 batch size. Our results that beat or match the standard training (the “released” model for FID and IS, and our reproduced results for Prec. and Rec.) are underlined.

Model	Method	Training Iter	Batch Size	NFE	FID(↓)	IS(↑)	Prec.(↑)	Rec.(↑)	Speed(↑)	
CD	EMA	50K	512	1	4.84	9.13	0.67	0.55		
		200K	512	1	4.08	9.18	0.68	0.56		
		400K	512	1	3.84	9.26	0.68	0.57		
		800K	512	1	3.66	9.35	0.68	0.57		
		800K	512	2	2.90	9.56	0.69	0.59		
		850K	512	1	3.65	9.32	0.68	0.57		
		850K	512	2	2.89	9.55	0.69	0.58		
		(released)	800K	512	1	3.55	9.48	-	-	
		(released)	800K	512	2	2.93	9.75	-	-	
		EMA*	800K	512	1	<u>3.51</u>	<u>9.37</u>	0.68	<u>0.57</u>	
LCSC	50K	512	1	<u>3.18</u>	<u>9.60</u>	0.67	<u>0.58</u>	~14×		
	250K	512	1	<u>2.76</u>	<u>9.71</u>	0.67	<u>0.59</u>	~3.1×		
	800K	512	1	<u>2.42</u>	9.76	0.67	<u>0.60</u>	-		
	800+40K	512	1	2.38	<u>9.70</u>	0.67	<u>0.60</u>	-		
	100K	128	1	<u>3.34</u>	<u>9.51</u>	0.67	<u>0.57</u>	~23×		
CT	EMA	200K	512	1	16.4	8.22	0.64	0.42		
		400K	512	1	12.1	8.52	0.67	0.43		
		600K	512	1	10.8	8.67	0.68	0.42		
		800K	512	1	9.87	8.81	0.69	0.42		
	(released)	800K	512	1	8.70	8.49	-	-		
	EMA*	800K	512	1	9.70	8.81	0.69	0.42		
	LCSC	400K	512	1	<u>8.60</u>	<u>8.89</u>	0.67	<u>0.47</u>	~1.9×	
800+40K	128	1	8.05	8.98	0.70	<u>0.45</u>	-			
450K	128	1	<u>8.33</u>	<u>8.67</u>	<u>0.69</u>	<u>0.44</u>	~7×			

For CM, on CIFAR-10 with CD, CT and ImageNet-64 with CD, to simulate scenarios where users have access only to pre-trained models, we fine-tune the final converged model for a few iterations and then apply LCSC. As illustrated in the 800+40K LCSC row with CD and CT in Tab. 1 and the 600+20K LCSC row with CD in Tab. 2, this approach significantly enhances the performance of the already converged model. For model developers, we directly utilize the checkpoints close to the final iteration, as demonstrated in the 800K LCSC row with CD in Tab. 1 and 1000K LCSC row with CT in Tab. 2. LCSC leads to notable improvements in all these scenarios. Notably, on CIFAR-10, LCSC even outperforms the 800K and 850K models that use 2-step sampling, achieving better performance with 1-step sampling (2.42, 2.38 FID vs. 2.89, 2.90 FID), thereby doubling the inference speed.

For DM, when applying LCSC at the final stage of training, we can identify a model that performs significantly better than the final model obtained through EMA, using the EMA rate selected by the baseline. While a better EMA model may be discovered through an extensive grid search, the outcomes

Table 2: Generation quality of consistency models on ImageNet-64. For CD, the speedup is compared against the standard training with 600K iterations and 2048 batch size. For CT, the speedup is compared against the standard training with 800K iterations and 2048 batch size. Our results that beat the standard training (“released”) are underlined.

Model	Method	Training Iter	Batch Size	NFE	FID(↓)	IS(↑)	Prec.(↑)	Rec.(↑)	Speed(↑)
CD	EMA	150K	256	1	8.24	36.2	0.66	0.61	
		300K	256	1	7.70	37.0	0.67	0.62	
		600K	256	1	7.30	37.2	0.67	0.62	
		650K	256	1	7.17	37.7	0.67	0.62	
		(released) 600K	2048	1	6.31	39.5	0.68	0.63	
		EMA*	600K	256	1	7.17	37.7	0.67	0.62
	LCSC	150K	256	1	6.56	38.9	0.67	0.62	~29×
		300K	256	1	<u>5.71</u>	41.8	<u>0.68</u>	0.62	~15×
		600+20K	256	1	5.54	<u>40.9</u>	<u>0.68</u>	0.62	~7.6×
CT	EMA	200K	256	1	20.3	28.8	0.61	0.53	
		400K	256	1	17.9	29.8	0.62	0.54	
		600K	256	1	16.6	30.6	0.62	0.54	
		800K	256	1	15.8	31.1	0.64	0.55	
		1000K	256	1	15.6	31.2	0.64	0.55	
		(released) 800K	2048	1	13.1	29.2	0.70	0.47	
	EMA*	1000K	256	1	15.6	31.2	0.64	0.55	
	LCSC	600K	256	1	<u>12.1</u>	<u>35.1</u>	0.67	<u>0.54</u>	~10.4×
		1000K	256	1	11.1	35.7	0.65	<u>0.57</u>	~6.3×

achieved by LCSC consistently surpass those obtained via the EMA strategy, thereby underscoring the superiority of our method. Moreover, we observe that the model identified through our approach can match the performance of the best EMA model with fewer NFE during inference. Specifically, on CIFAR-10, our method requiring NFE=9 is on par with EMA* using NFE=15. Similarly, on ImageNet-64, our method with NFE=12 is competitive with EMA* utilizing NFE=15. This highlights the potential for reducing inference costs while still achieving the baseline’s performance level.

5.3 Hyperparameter Study

The hyperparameters of LCSC includes the window size ($n_K - n_1$) for retrieving the historical weights, the interval ($n_k - n_{k-1}$) for two adjacent weight checkpoints, the number of samples for computing FID and the number of search iterations. Table 4 illustrates the impact of varying the number of samples, search iterations, and the size of the interval. We observe that increasing the number of samples and search iterations leads to higher performance, though this comes at the expense of increased search cost. In practice, we find that 10K samples and 2K search iterations can efficiently identify strong models. With a fixed window size, the interval between two checkpoints determines the dimension of the search space. Our findings suggest that search performance generally improves as the search space expands, but limiting the search dimension to fewer than 200 can detrimentally affect search performance. A more comprehensive study of the hyperparameters is provided in App. B.3.

Table 3: Generation quality of diffusion models. Our results that beat the standard training are underlined.

Dataset	Method	Training Iter.	NFE	FID(↓)	IS(↑)	Prec.(↑)	Rec.(↑)
CIFAR10	EMA	50K	15	80.9	5.51	0.52	0.30
		150K	15	<u>6.28</u>	8.74	0.61	0.59
		350K	15	4.45	9.23	0.63	0.59
		800K	15	4.16	9.37	0.64	0.60
	EMA*	800K	15	3.96	9.50	0.64	0.60
	LCSC	50K	15	10.8	8.35	0.55	0.58
		150K	15	4.76	8.97	0.61	0.59
		350K	15	<u>3.56</u>	9.35	0.64	0.60
		800K	15	3.18	9.59	0.64	<u>0.61</u>
		800K	12	<u>3.36</u>	<u>9.56</u>	0.64	0.60
800K		9	<u>3.97</u>	<u>9.50</u>	0.63	0.60	
ImageNet	EMA	50K	15	59.8	11.0	0.40	0.38
		150K	15	22.3	15.0	0.55	0.45
		350K	15	20.0	16.4	0.58	0.59
		500K	15	19.8	16.9	0.58	0.59
	EMA*	500K	15	18.1	17.3	0.59	0.59
	LCSC	50K	15	27.2	12.9	0.47	0.56
		150K	15	<u>19.1</u>	15.3	0.56	0.56
		350K	15	<u>16.8</u>	16.9	<u>0.59</u>	0.59
		500K	15	15.3	17.6	<u>0.59</u>	0.59
		500K	12	<u>17.2</u>	<u>17.2</u>	0.57	0.59
500K		10	20.5	<u>16.5</u>	0.55	0.58	

6 Discussion

In this section, we briefly discuss (1) Search results obtained by LCSC and (2) The reasons why LCSC performs better than traditional SGD.

Analysis of Search Patterns. We visualize several searched combination coefficients in Fig. 5. First, we observe a small subset of weights characterized by coefficients of large magnitude, whereas the coefficients for the majority of weights are nearly zero. This pattern suggests that the basin of the metric landscape likely occupies a subspace of lower rank compared to our entire search space. Additionally, the presence of multiple significant negative coefficients highlights that certain weights act as critical negative examples. This finding further implies that traditional weight averaging methods, such as EMA, are suboptimal, given that their results are confined to the convex hull of the weights, which excludes the discovered basin. More examples illustrating different scenarios are available in App. C.1.

LCSC vs. Gradient-based Methods. Our experiments in Sec. 5 have shown the promising benefits of LCSC. Specifically, it can find a basin in the metric landscape based on the weights obtained in early or middle training stages. An intriguing question arises regarding why gradient-based methods do not converge to the basin found by LCSC. In this work, we offer some insights from our research and defer a more comprehensive theoretical investigation to future studies. First, the objective of LCSC is different from gradient-based method.

Table 4: Hyperparameter study of LCSC with (a) DM and (b) CM. The models are trained on CIFAR10 with 250K iterations. We evaluate three values of each hyperparameter and compare them with our adopted setting highlighted in gray. The varied hyperparameter is in bold. For DM the window size is 50K, for CM it is 40K.

(a) Results on DM					(b) Results on CM				
Samples	Search	Iters.	Interval FID(\downarrow)	IS(\uparrow)	Samples	Search	Iters.	Interval FID(\downarrow)	IS(\uparrow)
10K	2K	200	3.87	9.27	10K	2K	100	2.76	9.71
2K	2K	200	9.23	9.11	2K	2K	100	3.40	9.39
5K	2K	200	4.04	9.09	5K	2K	100	2.79	9.66
10K	1K	200	4.01	9.17	10K	1K	100	3.03	9.57
10K	4K	200	3.79	9.28	10K	4K	100	2.69	9.70
10K	2K	100	3.82	9.15	10K	2K	200	2.84	9.71
10K	2K	500	4.41	9.11	10K	2K	50	2.71	9.79

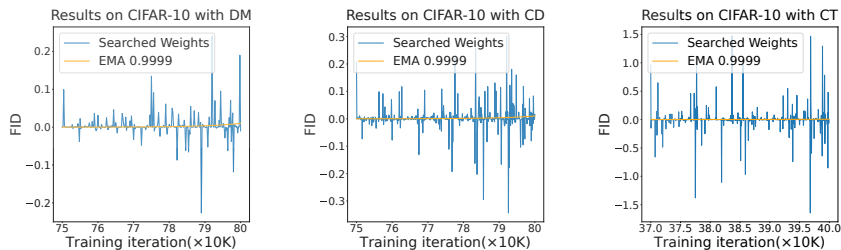


Fig. 5: Visualization of weight combination coefficients obtained using LCSC compared to those from the default EMA on CIFAR10.

In this work, we employ FID as the search objective as it turns out to be efficient. In principle LCSC can search any objective while gradient-based methods require the objective to be differentiable. It is worth noting that minimizing ℓ_2 loss, which is commonly used in gradient-based optimization, does not necessarily lead to higher generation quality [21, 44]. Second, DM and CM have a large variance in their gradient estimation as discussed in Sec. 3. During training, they may not be able to stay stationary within the basin we have found if the basin is small. A more detailed discussion is provided in App. C.1.

7 Conclusion

This work proposes a simple but effective method, LCSC, to enhance the training process of DMs and CMs. Based on observations of the metric landscape, we propose to linearly combine saved checkpoints during training to achieve better performance. We further use evolutionary search to find the optimal group of combination coefficients. Our method can be used to decrease the training iteration and batch size, or enhance the final converged models.

Acknowledgement

This work was supported by National Natural Science Foundation of China (No. 62325405, 62104128, U19B2019, U21B2031, 61832007, 62204164), Flemish Government (AI Research Program) and the Research Foundation - Flanders (FWO) through project number G0G2921N, Tsinghua EE Xilinx AI Research Fund, and Beijing National Research Center for Information Science and Technology (BN-Rist). We thank for all the support from Infinigence-AI.

References

1. Berthelot, D., Autef, A., Lin, J., Yap, D.A., Zhai, S., Hu, S., Zheng, D., Talbott, W., Gu, E.: Tract: Denoising diffusion models with transitive closure time-distillation. arXiv preprint arXiv:2303.04248 (2023)
2. Blattmann, A., Dockhorn, T., Kulal, S., Mendelevitch, D., Kilian, M., Lorenz, D., Levi, Y., English, Z., Voleti, V., Letts, A., et al.: Stable video diffusion: Scaling latent video diffusion models to large datasets. arXiv preprint arXiv:2311.15127 (2023)
3. Deng, J., Dong, W., Socher, R., Li, L.J., Li, K., Fei-Fei, L.: Imagenet: A large-scale hierarchical image database. In: 2009 IEEE conference on computer vision and pattern recognition. pp. 248–255. Ieee (2009)
4. Dhariwal, P., Nichol, A.: Diffusion models beat gans on image synthesis. *Advances in Neural Information Processing Systems* **34**, 8780–8794 (2021)
5. Go, H., Lee, Y., Lee, S., Oh, S., Moon, H., Choi, S.: Addressing negative transfer in diffusion models. *Advances in Neural Information Processing Systems* **36** (2024)
6. Hang, T., Gu, S., Li, C., Bao, J., Chen, D., Hu, H., Geng, X., Guo, B.: Efficient diffusion training via min-snr weighting strategy. In: *Proceedings of the IEEE/CVF International Conference on Computer Vision*. pp. 7441–7451 (2023)
7. Heusel, M., Ramsauer, H., Unterthiner, T., Nessler, B., Hochreiter, S.: Gans trained by a two time-scale update rule converge to a local nash equilibrium. *Advances in neural information processing systems* **30** (2017)
8. Ho, J., Jain, A., Abbeel, P.: Denoising diffusion probabilistic models. *Advances in Neural Information Processing Systems* **33**, 6840–6851 (2020)
9. Ho, J., Salimans, T., Gritsenko, A., Chan, W., Norouzi, M., Fleet, D.J.: Video diffusion models. arXiv preprint arXiv:2204.03458 (2022)
10. Hyvärinen, A.: Estimation of non-normalized statistical models by score matching. *Journal of Machine Learning Research* **6**(24), 695–709 (2005)
11. Ilharco, G., Ribeiro, M.T., Wortsman, M., Gururangan, S., Schmidt, L., Hajishirzi, H., Farhadi, A.: Editing models with task arithmetic. arXiv preprint arXiv:2212.04089 (2022)
12. Izmailov, P., Podoprikin, D., Garipov, T., Vetrov, D., Wilson, A.: Averaging weights leads to wider optima and better generalization. In: Silva, R., Globerson, A., Globerson, A. (eds.) *34th Conference on Uncertainty in Artificial Intelligence 2018, UAI 2018*. pp. 876–885. *34th Conference on Uncertainty in Artificial Intelligence 2018, UAI 2018, Association For Uncertainty in Artificial Intelligence (AUAI)* (2018)
13. Jin, X., Ren, X., Preotiuc-Pietro, D., Cheng, P.: Dataless knowledge fusion by merging weights of language models. arXiv preprint arXiv:2212.09849 (2022)
14. Jolicœur-Martineau, A., Li, K., Piché-Taillefer, R., Kachman, T., Mitliagkas, I.: Gotta go fast when generating data with score-based models. arXiv preprint arXiv:2105.14080 (2021)
15. Karras, T., Aittala, M., Aila, T., Laine, S.: Elucidating the design space of diffusion-based generative models. *Advances in Neural Information Processing Systems* **35**, 26565–26577 (2022)
16. Kingma, D.P., Ba, J.: Adam: A method for stochastic optimization. arXiv preprint arXiv:1412.6980 (2014)
17. Krizhevsky, A., Hinton, G., et al.: Learning multiple layers of features from tiny images (2009)

18. Kynkäänniemi, T., Karras, T., Laine, S., Lehtinen, J., Aila, T.: Improved precision and recall metric for assessing generative models. *Advances in Neural Information Processing Systems* **32** (2019)
19. Li, L., Li, H., Zheng, X., Wu, J., Xiao, X., Wang, R., Zheng, M., Pan, X., Chao, F., Ji, R.: Autodiffusion: Training-free optimization of time steps and architectures for automated diffusion model acceleration. In: *Proceedings of the IEEE/CVF International Conference on Computer Vision*. pp. 7105–7114 (2023)
20. Lin, C.H., Gao, J., Tang, L., Takikawa, T., Zeng, X., Huang, X., Kreis, K., Fidler, S., Liu, M.Y., Lin, T.Y.: Magic3d: High-resolution text-to-3d content creation. In: *Proceedings of the IEEE/CVF Conference on Computer Vision and Pattern Recognition*. pp. 300–309 (2023)
21. Liu, E., Ning, X., Lin, Z., Yang, H., Wang, Y.: Oms-dpm: Optimizing the model schedule for diffusion probabilistic models. *arXiv preprint arXiv:2306.08860* (2023)
22. Liu, E., Ning, X., Yang, H., Wang, Y.: A unified sampling framework for solver searching of diffusion probabilistic models. *arXiv preprint arXiv:2312.07243* (2023)
23. Liu, L., Ren, Y., Lin, Z., Zhao, Z.: Pseudo numerical methods for diffusion models on manifolds. In: *International Conference on Learning Representations* (2022), <https://openreview.net/forum?id=P1KWVd2yBkY>
24. Lu, C., Zhou, Y., Bao, F., Chen, J., Li, C., Zhu, J.: Dpm-solver: A fast ode solver for diffusion probabilistic model sampling in around 10 steps. *arXiv preprint arXiv:2206.00927* (2022)
25. Luo, S., Tan, Y., Huang, L., Li, J., Zhao, H.: Latent consistency models: Synthesizing high-resolution images with few-step inference. *arXiv preprint arXiv:2310.04378* (2023)
26. Luo, S., Tan, Y., Patil, S., Gu, D., von Platen, P., Passos, A., Huang, L., Li, J., Zhao, H.: Lcm-lora: A universal stable-diffusion acceleration module. *arXiv preprint arXiv:2311.05556* (2023)
27. Malladi, S., Gao, T., Nichani, E., Damian, A., Lee, J.D., Chen, D., Arora, S.: Fine-tuning language models with just forward passes. *Advances in Neural Information Processing Systems* **36** (2024)
28. Nichol, A.Q., Dhariwal, P.: Improved denoising diffusion probabilistic models. In: Meila, M., Zhang, T. (eds.) *Proceedings of the 38th International Conference on Machine Learning*. *Proceedings of Machine Learning Research*, vol. 139, pp. 8162–8171. PMLR (18–24 Jul 2021)
29. Ning, X., Zheng, Y., Zhao, T., Wang, Y., Yang, H.: A generic graph-based neural architecture encoding scheme for predictor-based nas. In: *European Conference on Computer Vision*. pp. 189–204. Springer (2020)
30. Polyak, B.T., Juditsky, A.B.: Acceleration of stochastic approximation by averaging. *SIAM Journal on Control and Optimization* **30**(4), 838–855 (1992)
31. Poole, B., Jain, A., Barron, J.T., Mildenhall, B.: Dreamfusion: Text-to-3d using 2d diffusion. *arXiv preprint arXiv:2209.14988* (2022)
32. Real, E., Aggarwal, A., Huang, Y., Le, Q.V.: Regularized evolution for image classifier architecture search. In: *Proceedings of the aaai conference on artificial intelligence*. vol. 33, pp. 4780–4789 (2019)
33. Rombach, R., Blattmann, A., Lorenz, D., Esser, P., Ommer, B.: High-resolution image synthesis with latent diffusion models. In: *Proceedings of the IEEE/CVF Conference on Computer Vision and Pattern Recognition*. pp. 10684–10695 (2022)
34. Ruppert, D.: Efficient estimations from a slowly convergent robbins-monro process. Technical report, Cornell University Operations Research and Industrial Engineering (1988)

35. Salimans, T., Goodfellow, I., Zaremba, W., Cheung, V., Radford, A., Chen, X.: Improved techniques for training gans. *Advances in neural information processing systems* **29** (2016)
36. Sohl-Dickstein, J., Weiss, E., Maheswaranathan, N., Ganguli, S.: Deep unsupervised learning using nonequilibrium thermodynamics. In: *International Conference on Machine Learning*. pp. 2256–2265. PMLR (2015)
37. Song, J., Meng, C., Ermon, S.: Denoising diffusion implicit models. arXiv:2010.02502 (October 2020), <https://arxiv.org/abs/2010.02502>
38. Song, Y., Dhariwal, P.: Improved techniques for training consistency models. In: *The Twelfth International Conference on Learning Representations* (2024)
39. Song, Y., Dhariwal, P., Chen, M., Sutskever, I.: Consistency models. arXiv preprint arXiv:2303.01469 (2023)
40. Song, Y., Sohl-Dickstein, J., Kingma, D.P., Kumar, A., Ermon, S., Poole, B.: Score-based generative modeling through stochastic differential equations. arXiv preprint arXiv:2011.13456 (2020)
41. Spall, J.C.: Multivariate stochastic approximation using a simultaneous perturbation gradient approximation. *IEEE transactions on automatic control* **37**(3), 332–341 (1992)
42. Szegedy, C., Vanhoucke, V., Ioffe, S., Shlens, J., Wojna, Z.: Rethinking the inception architecture for computer vision. In: *Proceedings of the IEEE conference on computer vision and pattern recognition*. pp. 2818–2826 (2016)
43. Wang, X., Zhang, S., Zhang, H., Liu, Y., Zhang, Y., Gao, C., Sang, N.: Videolcm: Video latent consistency model. arXiv preprint arXiv:2312.09109 (2023)
44. Watson, D., Ho, J., Norouzi, M., Chan, W.: Learning to efficiently sample from diffusion probabilistic models. arXiv preprint arXiv:2106.03802 (2021)
45. Wortsman, M., Ilharco, G., Gadre, S.Y., Roelofs, R., Gontijo-Lopes, R., Morcos, A.S., Namkoong, H., Farhadi, A., Carmon, Y., Kornblith, S., Schmidt, L.: Model soups: averaging weights of multiple fine-tuned models improves accuracy without increasing inference time. In: Chaudhuri, K., Jegelka, S., Song, L., Szepesvari, C., Niu, G., Sabato, S. (eds.) *Proceedings of the 39th International Conference on Machine Learning*. *Proceedings of Machine Learning Research*, vol. 162, pp. 23965–23998. PMLR (17–23 Jul 2022)
46. Yadav, P., Tam, D., Choshen, L., Raffel, C.A., Bansal, M.: Ties-merging: Resolving interference when merging models. *Advances in Neural Information Processing Systems* **36** (2024)
47. Yang, S., Chen, Y., Wang, L., Liu, S., Chen, Y.: Denoising diffusion step-aware models. arXiv preprint arXiv:2310.03337 (2023)
48. Yu, L., Yu, B., Yu, H., Huang, F., Li, Y.: Language models are super mario: Absorbing abilities from homologous models as a free lunch. arXiv preprint arXiv:2311.03099 (2023)
49. Zhang, R., Isola, P., Efros, A.A., Shechtman, E., Wang, O.: The unreasonable effectiveness of deep features as a perceptual metric. In: *2018 IEEE/CVF Conference on Computer Vision and Pattern Recognition (CVPR)*. pp. 586–595. IEEE Computer Society (2018)

APPENDIX

Linear Combination of Saved Checkpoints Makes Consistency and Diffusion Models Better

In this appendix, we provide additional examples of the metric landscape in App. A. We further elaborate on our experimental setup and present additional results in App. B. A more in-depth discussion of our work is provided in App. C. Potential directions for future work are explored in App. D. Finally, we offer visualizations of the generated images in App. E. We will open-source our code to promote the application of LCSC.

A Additional Examples of the Metric Landscape

We previously introduced the metric landscape of the DM and CD models in Sec. 3. In this section, we extend our analysis by evaluating additional metric landscapes using the FID. Specifically, we incorporate an additional intermediate training iteration and explore the metric landscape of the CT model. The comprehensive landscapes of the DM, CD, and CT models are depicted in Fig. 6.

B Experimental Details and Additional Results

B.1 Experimental Details

Training Setting Since LCSC employs weight checkpoints, we endeavored to replicate the training processes of the baseline models. For DMs, we were able to reproduce the results reported in the original papers successfully. However, for CMs, our training outcomes on CIFAR10 were slightly inferior to those documented in the original papers. Additionally, due to resource constraints, we opted for a smaller batch size than the original configuration when training on ImageNet. In the results tables, we present both our training outcomes and the results reported in the original papers, with the latter indicated as *released*. The specifics of the experimental setups are detailed below.

For the experiments with DM, we utilize the DDIM [37] codebase (<https://github.com/ermongroup/ddim>) on CIFAR-10, adhering to the default configuration settings. For ImageNet-64, we employ the iDDPM [28] codebase (<https://github.com/openai/improved-diffusion>), setting the batch size to 512, the noise schedule to cosine, and maintaining other hyperparameters at their default values. During sampling, the DPM-Solver [24] (<https://github.com/LuChengTHU/dpm-solver>) is applied, conducting 15 timesteps of denoising using the default configuration for the respective setting. The reproduced results are on par with or slightly surpass those achieved using Euler integration, as reported in the original papers.

For the experiments involving CM, we adhere closely to the configurations detailed in Table 3 of the original CM paper [39]. On CIFAR-10, instead of using the NCSNPP model [40] from CM’s official implementation, we opt for the EDM [15]

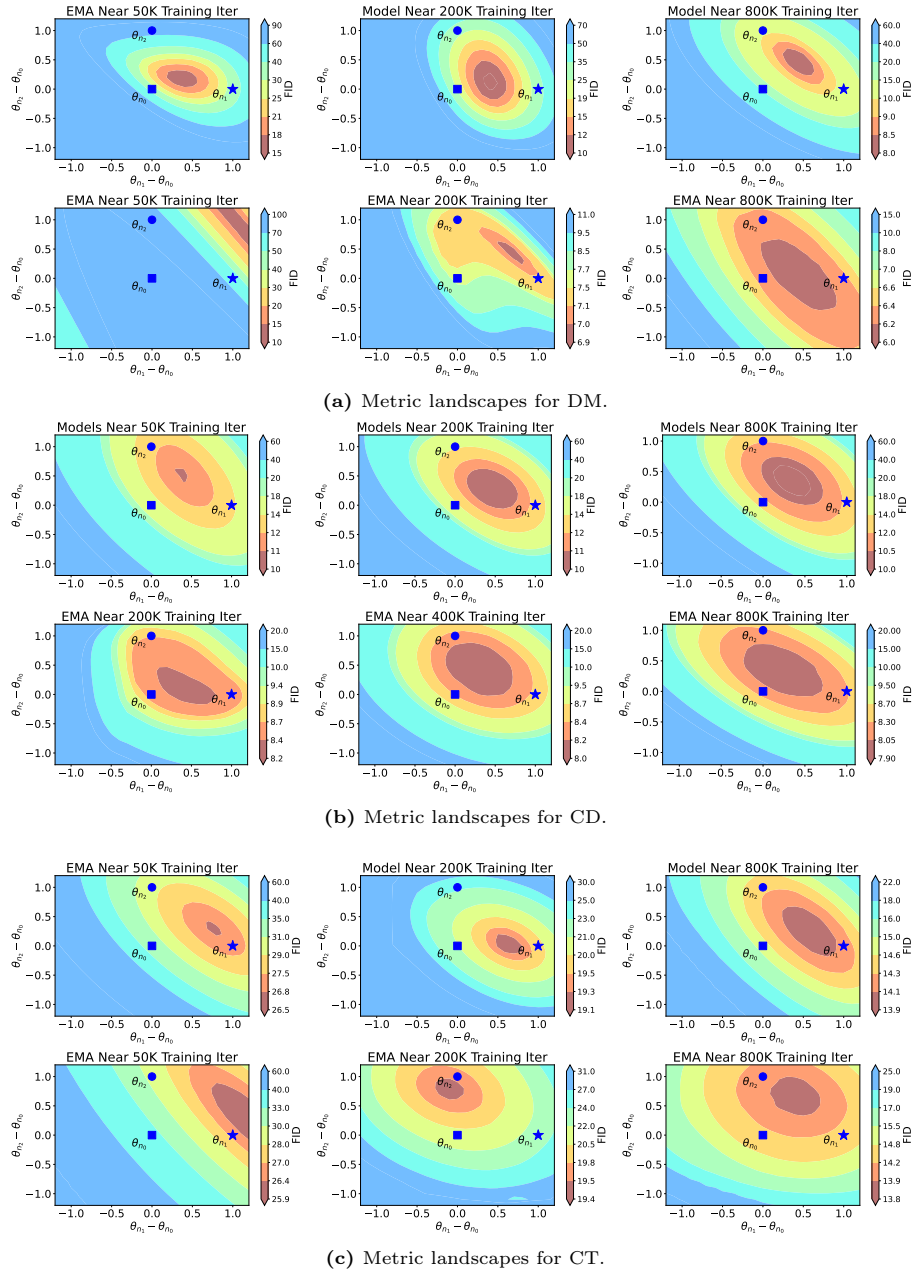


Fig. 6: Metric landscapes for DM, CD and CT on CIFAR-10.

architecture. This decision stems from the official CM code for CIFAR-10 being implemented in JAX while our experiments are conducted using PyTorch. For

Table 5: Search time consumption per search iteration (in seconds). Results marked with * denote the CPU time cost, which is excludable from the overall time cost through parallel processing. “U-Net” refers to the denoising sampling process, “Inception” refers to the computation of inception features, “Merging” refers to the averaging of weights, and “FID” refers to the computation of FID statistics.

Model	Dataset	U-Net	Inception	Merging*	FID*
CM	CIFAR-10	7.34	4.28	5.57	2.49
	ImageNet-64	34.7	4.32	12.0	2.37
DM	CIFAR-10	40.9	4.39	4.61	2.49
	ImageNet-64	114.5	2.24	13.8	2.53

further details, refer to https://github.com/openai/consistency_models_cifar10. This difference in implementation may partly explain the discrepancies between our replication results and those reported in Table 1 of CM’s original paper [39]. On ImageNet-64, we follow the official implementation, employing the ADM [4] architecture. Due to resource constraints, we train the model with a smaller batch size of 256 instead of 2048 as used in the original study, resulting in worse outcomes. However, as indicated in Tab. 2, applying LCSC to models trained with a reduced batch size can still achieve performance comparable to models trained with a larger batch size.

Search Setting At each selected training iteration, historical weights are leveraged within designated window sizes and intervals. For CM, checkpoints have a window size of 40K with an interval of 100 on CIFAR-10, and a window size of 20K with an interval of 100 on ImageNet-64. DM is assigned a window size of 50K and an interval of 200 for both datasets. FID calculation for DM on ImageNet-64 utilizes a sample of 5K images, while 10K images are used for all other configurations. An evolutionary search spanning 2K iterations is applied consistently across all experimental setups.

B.2 Search Cost Estimation

We detail the estimation of search costs, covering both CPU and GPU time consumption. Saved checkpoints are loaded into CPU memory and then transferred to the GPU after averaging. Consequently, CPU time comprises the duration for merging weight checkpoints and calculating the FID statistic. Meanwhile, GPU time is dedicated to the sampling and evaluation processes involving the diffusion U-Net and the Inception network. All experiments are performed on a single NVIDIA A100 GPU, paired with an Intel Xeon Platinum 8385P CPU.

First, we profile the durations of each function across all experimental settings and document the time consumed in a single search iteration in Tab. 5. We note that the CPU time cost is significantly lower than that on the GPU. Therefore, while conducting sampling with the current merged weights on the GPU, we

Table 6: Overall search time and training time consumption (in hours).

Model	Dataset	Search		Training		
		Iteration	Time	Iteration	Batch Size	Time
CD	CIFAR-10	2K	6.45	800K	512	818
	ImageNet-64	2K	21.7	600K	2048	7253
CT	CIFAR-10	2K	6.45	800K	512	640
	ImageNet-64	2K	21.7	800K	2048	7040
DM	CIFAR-10	2K	25.2	800K	128	29.3
	ImageNet-64	2K	64.8	500K	512	372

Table 7: Accurate training speedup of consistency models on CIFAR-10. The speedup is compared against the standard training with 800K iterations and 512 batch size.

Model	Method	Training Iter	Batch Size	Speedup(\uparrow)
CD	EMA	800K	512	-
	LCSC	50K	512	14.27 \times
		250K	512	3.12 \times
		100K	128	25.55 \times
CT	EMA (released)	800K	512	-
	LCSC	400K	512	1.96 \times
		450K	128	6.64 \times

can simultaneously perform the FID statistic computation from the previous iteration and merge the checkpoints for the next iteration on the CPU. As a result, the CPU time cost can be effectively excluded from the overall time cost.

Next, we examine the overall training and search time costs as outlined in Tab. 6, and we delve into the speedup ratio detailed in Tabs. 7 and 8. Given that DMs necessitate multiple timesteps for sampling, the overall search cost for DM proves to be non-negligible when compared to the training cost. This results in no observable speedup in convergence upon applying LCSC. However, this search cost is considered manageable and warranted for the anticipated improvements to the final model convergence.

In contrast, for CMs, the search cost is substantially lower than the training cost, which often results in a markedly faster convergence when combining training with LCSC than with training alone. The precise speedup ratios for CM training are detailed in Tabs. 7 and 8. It should be noted that the figures in these tables may exhibit slight discrepancies from those reported in Sec. 5 due to the latter being profiled in an environment with more variables and potential fluctuations.

Table 8: Accurate training speedup of consistency models on ImageNet-64. For CD, the speedup is compared against standard training with 600K iterations and 2048 batch size. For CT, the speedup is compared against standard training with 800K iterations and 2048 batch size.

Model	Method	Training Iter	Batch Size	Speedup(\uparrow)
CD	EMA (released)	600K	2048	-
	LCSC	150K	256	29.20 \times
		300K	256	15.27 \times
		620K	256	7.55 \times
CT	EMA (released)	800K	2048	-
	LCSC	600K	256	10.33 \times
		1000K	256	6.27 \times

B.3 Hyperparameter Study

In Sec. 5.3, we investigate the sensitivity of several hyperparameters, including the number of search iterations, the number of samples, and the interval between two weight checkpoints ($n_k - n_{k-1}$). This section focuses on the impact of window size ($n_K - n_1$) on the performance of our search algorithm. Given that DM operates iteratively during sampling and a larger NFE (i.e. the number of timesteps for the ODE solver) typically leads to higher generation quality, we also examine the effects of varying NFE during the search within the DM context. The findings are detailed in Table 9.

The results reveal that, despite earlier models being further from convergence, a sufficiently large window for accessing historical weights proves advantageous. Furthermore, conducting a lower NFE during the search in the DM context results in a similar reduction in FID but a smaller improvement in IS. This suggests that the search output’s generality across different metrics diminishes when the generated samples during the search are less accurate, i.e., exhibit significant truncation error.

B.4 Detailed Results of EMA Rate Grid Search

For the final training model of each experimental configuration, we conduct a comprehensive sweep across a broad range of EMA rates, presenting the optimal outcomes in Sec. 5. The exhaustive results are detailed in Tab. 10. In the majority of scenarios, the default EMA rate employed in the official implementations of our baseline models [8, 28, 39] yields slightly inferior performance compared to the best EMA rate identified. Nevertheless, the findings demonstrate that LCSC consistently surpasses all explored EMA rates, underscoring the limitations of EMA as a strategy for weight averaging.

Table 9: Hyperparameter analysis of LCSC, supplementing the study in Tab. 4. Models are trained on CIFAR10 for 250K iterations. We assess three different values for each hyperparameter, contrasting these with our chosen setting, which is highlighted in gray. The hyperparameter under variation is indicated in bold. For DM, the interval between checkpoints is set to 200, whereas for CM, it is 100. We perform 2K search iterations and sample 10K images to compute the FID score at each iteration.

Method	Window Size	NFE	FID(↓)	IS(↑)
CM	40K	1	2.76	9.71
	10K	1	2.89	9.60
	50K	1	2.73	9.66
DM	50K	15	3.87	9.27
	10K	15	4.41	9.11
	30K	15	3.82	9.15
	50K	7	3.91	9.10
	50K	10	3.84	9.17

Table 10: EMA rate grid search outcomes. Asterisks (*) indicate the results using the default rates from the official paper. Listed FID scores for each EMA rate correspond to fully trained models: CIFAR-10 models at 800K iterations; ImageNet-64 CD/CT/DM models at 600K/1000K/500K iterations, respectively. Iteration counts for models employed by LCSC are shown in parentheses.

Model	Dataset	EMA rate							LCSC
		0.999	0.9995	0.9999	0.999943	0.99995	0.99997	0.99999	
CD	CIFAR-10	4.35	4.13	3.66*	3.56	3.58	3.51	3.54	2.42 (800K)
	ImageNet-64	7.45	7.38	7.19	7.17*	7.17	7.22	7.41	5.54 (620K)
CT	CIFAR-10	9.80	9.78	9.70*	9.70	9.69	9.71	9.77	8.60 (400K)
	ImageNet-64	15.7	15.7	15.6	15.6*	15.6	15.6	15.7	12.1 (600K)
DM	CIFAR-10	5.73	5.18	4.16*	3.99	3.96	4.04	5.04	3.18 (800K)
	ImageNet-64	23.1	20.3	19.8*	19.0	18.1	18.1	18.5	15.3 (500K)

B.5 Evaluation with FID@CLIP

In this section, we present the results of FID@CLIP (i.e., FID computed within the feature space of a CLIP model) to demonstrate that LCSC facilitates improvements beyond the inception feature space. We utilize the visual component of a CLIP model based on ViT-B/32. Detailed outcomes are documented in Tabs. 11 and 12. The findings clearly indicate that LCSC consistently surpasses the performance of the EMA, as measured by FID@CLIP. Notably, models trained for fewer iterations or with smaller batch sizes experience enhancements through LCSC, achieving better performance than the fully converged EMA model as gauged by FID@CLIP.

Table 11: FID on CIFAR10 calculated within the visual feature space of a CLIP model, denoted as FID@CLIP.

Model	Method	Training Iter	Batch Size	NFE	FID(↓)	FID@CLIP(↓)	
CD	EMA	50K	512	1	4.84	28.1	
		250K	512	1	4.08	20.3	
		800K	512	1	3.66	17.7	
		800K	512	2	2.90	13.3	
		850K	512	1	3.65	17.3	
		850K	512	2	2.89	13.1	
	LCSC	50K	512	1	3.18	21.4	
		250K	512	1	2.76	14.3	
		800K	512	1	2.42	14.8	
		800+40K	512	1	2.38	14.1	
	CT	EMA	400K	512	1	12.08	43.0
			800K	512	1	9.87	35.8
LCSC		400K	512	1	8.60	29.5	
		450K	128	1	8.33	25.5	
DM	EMA	150K	128	15	6.28	46.4	
		350K	128	15	4.45	41.9	
		800K	128	15	4.16	42.7	
	LCSC	150K	128	15	4.76	43.1	
		350K	128	15	3.56	36.1	
		800K	128	15	3.18	36.4	

C More Insights and Analysis

C.1 Analysis of Search Patterns

More Examples of Search Patterns We demonstrate search results on ImageNet-64 in Fig. 7, which share similar patterns with results on CIFAR-10 (refer to Fig. 5). Our analysis in Sec. 6 also holds in these cases.

Consistency of Search Results We evaluate the consistency of search patterns by comparing results across different random seeds. As indicated in Tab. 13, both seeds produce similar outcomes in terms of FID and IS metrics. Yet, Fig. 8 reveals that each seed’s dominant coefficients map to distinct subsets of weight checkpoints, suggesting the presence of multiple high-quality basins within the weight checkpoint subspace. This diversity underscores LCSC’s ability to identify and enhance model performance within one of these basins through a limited number of search iterations (e.g., 2K in our experiments), demonstrating its efficiency and effectiveness.

Table 12: FID on ImageNet-64 calculated within the visual feature space of a CLIP model, denoted as FID@CLIP.

Model	Method	Training Iter	Batch Size	NFE	FID(↓)	FID@CLIP(↓)
CD	(released)	300K	256	1	7.70	30.0
		600K	256	1	7.30	29.1
		650K	256	1	7.17	28.4
		600K	2048	1	6.31	25.5
	LCSC	300K	256	1	5.71	28.2
		600+20K	256	1	5.54	24.9
CT	(released)	600K	256	1	16.6	49.8
		1000K	256	1	15.6	47.5
		800K	2048	1	13.1	47.5
	LCSC	600K	256	1	12.1	38.3
DM	EMA	250K	512	15	20.8	46.6
		500K	512	15	19.8	44.2
	LCSC	250K	512	15	16.3	44.8
		500K	512	15	15.3	41.5

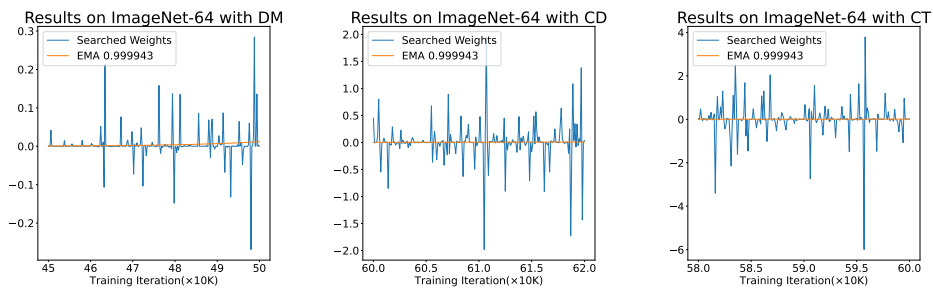


Fig. 7: Visualization of weight combination coefficients obtained using LCSC compared to those from the default EMA on ImageNet-64.

Table 13: Performance of LCSC with different random seeds.

Model	Method	Training Iter	Batch Size	NFE	Seed	FID(↓)	IS(↑)
CD	LCSC	250K	512	1	1	2.76	9.71
					2	2.69	9.69

The Critical Role of Search Space Configuration As explored in Sec. 6, restricting averaged weights to the convex hull of candidate checkpoints, where all combination coefficients are non-negative and their sum equals 1, might limit search efficacy. To test this hypothesis, we perform searches under convex combination conditions by clipping coefficients to non-negative values and normalizing

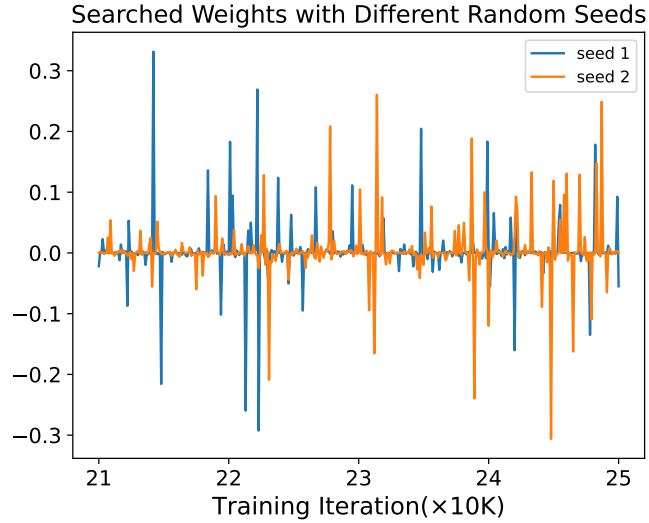


Fig. 8: Visualization of linear combination coefficients obtained by LCSC with different random seeds.

Table 14: Performance of LCSC with or without restriction to the convex hull of all saved checkpoints. “w/o” in the column “Restriction” is our default setting in main experiments, while “w” means the restriction holds.

Model	Method	Training Iter	Batch Size	NFE	Restriction	FID(↓)	IS(↑)
CD	LCSC	250K	512	1	w/o	2.76	9.71
					w	3.38	9.36
DM	LCSC	350K	128	15	w/o	3.56	9.35
					w	3.59	9.29

their sum to 1. Table 14 presents these findings, with “w/o” indicating no restriction on coefficients (allowing values below zero) and “w” representing the convex hull restriction. The results clearly show superior performance without the convex restriction, underscoring its limiting effect on search outcomes. Furthermore, we discover that normalizing the coefficient sum to 1 is vital for effective search exploration, a practice we continue even after lifting the convex condition, as detailed in Eq. (7).

C.2 Discussion on the Training Variance of DM and CM

As discussed in Sec. 3, we are motivated by the observation that the training objectives of DM and CM tend to introduce substantial variance in gradient

estimations. We further discuss the potential reasons or hypothesis of such phenomenon as follows.

Unbiased Estimation as Objective The objectives used in DM and CT are not accurate for any single batch. Instead, they serve as an unbiased estimation. Specifically, for DM, the neural network learns the score function at any (\mathbf{x}_t, t) , denoted as $\mathbf{s}_\theta(\mathbf{x}_t, t)$. The ground truth score function $\nabla \log p_t(\mathbf{x}_t)$ is given as [40]:

$$\nabla \log p_t(\mathbf{x}_t) = \mathbb{E}_{\mathbf{y} \sim p_{\text{data}}, \varepsilon \sim \mathcal{N}(\mathbf{0}, \sigma(t)^2 \mathbf{I})} \left(-\frac{\varepsilon}{\sigma_t} \mid \alpha_t \mathbf{y} + \sigma_t \varepsilon = \mathbf{x}_t \right) \quad (8)$$

This formula implies that every sample \mathbf{y} in the dataset contributes to the ground truth score function at any (\mathbf{x}_t, t) . However, the training objective Eq. (3) provides only an unbiased estimation of the ground truth score Eq. (8). At every iteration, the current target for the network is not identical to the ground truth score function but is determined by the sample \mathbf{y} randomly drawn from the dataset and the noise level σ_t . Thus, even if $\mathbf{s}_\theta(\mathbf{x}_t, t)$ exactly matches $\nabla p_t(\mathbf{x}_t)$ for $\forall(\mathbf{x}_t, t)$, its gradient estimation using a mini-batch of data does not converge to zero. The approximation of ground truth score function can only be obtained through the expectation over many training iterations. For CT, the situation is very similar. To simulate the current ODE solution step without a teacher diffusion model, Song et al. [39] utilize the Monte Carol estimation $-\frac{\mathbf{x}_t - \mathbf{y}}{t^2}$ to replace the ground truth score function $\nabla \log p_t(\mathbf{x}_t) = \mathbb{E}_{\mathbf{y} \sim p_{\text{data}}, \mathbf{x}_t \sim \mathcal{N}(\mathbf{y}, t^2 \mathbf{I})} \left(-\frac{\mathbf{x}_t - \mathbf{y}}{t^2} \mid \mathbf{x}_t \right)$ under the noise schedule from EDM [15] as denoted in Eq. (5). Therefore, the objective is also not accurate for any single batch of data and the model has to learn to fit the target model output after solving the current step with the expectation of score function among many training iterations. These types of objectives, which are not accurate for any single batch, introduce high variance to the gradient estimation.

Model across Different Time steps For both DM and CM, the neural network has to be trained at various time steps. Since the model input and output follow different distributions, the gradients at different time steps may conflict with each other. This phenomenon of negative transfer between timesteps has been studied in several previous work, where they train different diffusion neural networks at different timesteps and achieve better performance [5, 6]. The misalignment between the objectives of different time steps may also contribute to the high variance in the gradient estimation.

Error Accumulation of CM For CM, the model learns to approximate the output of the target model at the previous step. This could potentially introduce the problem of error accumulation [1]. Consequently, any noise introduced during training at early time steps is likely to lead to inaccuracies in the target model, which may be magnified in subsequent timesteps. This property of CM amplifies the high training variance, particularly for one-step sampling.

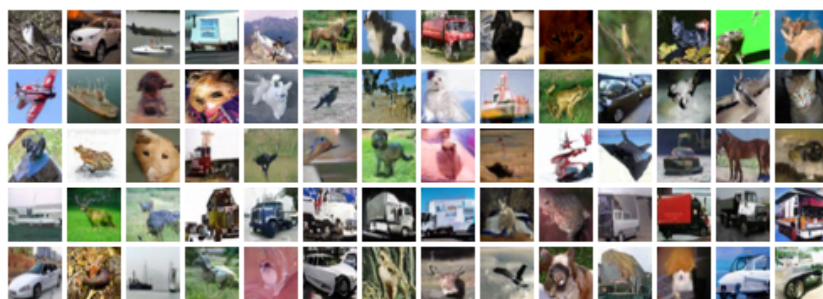
D Future Work

LCSC represents a novel optimization paradigm, indicating its potential for widespread application. We recommend future investigations focus on three key areas:

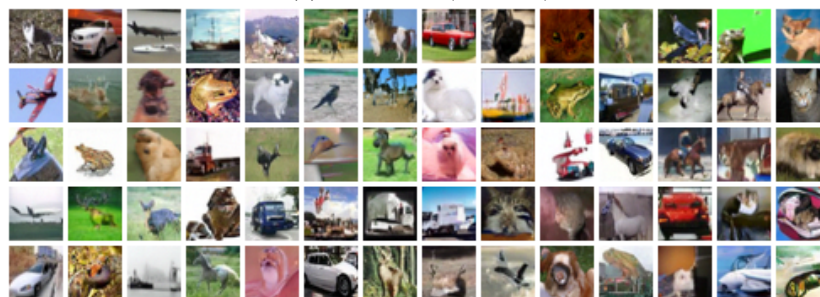
- *Expanded Search Space:* Presently, LCSC applies a uniform coefficient across an entire model. Considering that different model layers might benefit from distinct combination coefficients, partitioning model weights into segments for unique coefficient assignments could enhance the search space. For DMs, adopting variable coefficients across different timesteps may also offer further improvements.
- *Efficient Optimization Methods:* The current reliance on evolutionary methods, characterized by their dependency on randomness, limits efficiency and risks convergence to local optima. Investigating more effective optimization strategies presents a promising avenue for enhancing LCSC.
- *Broader Application Scope:* While the initial motivation for LCSC stems from managing the high training variance observed in DMs and CMs, its utility is not confined to these models. Exploring LCSC’s applicability to other domains, such as fine-tuning language models or additional vision models, could unlock new performance gains.

E Visualization

In this section, visualizations of images generated by DM (Figs. 9 and 10), CD (Figs. 11 and 12), and CT (Figs. 13 and 14) are presented. Many images produced by the EMA model are observed to be similar to those produced by the model derived from our LCSC when using the same noise input. This is expected given that both models are based on weights from the same training cycle. To more clearly highlight the distinctions between EMA and LCSC, we generate 50K images from EMA and LCSC using the same set of noise inputs, order the image pairs according to their Euclidean distances in the inception feature space, and randomly select the images with large distances. In general, images generated by the LCSC model are found to display enhanced sharpness, diminished noise, and more distinct object representation.

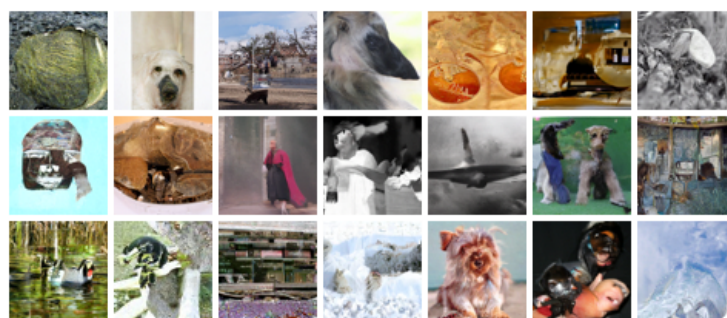


(a) EMA model (FID: 4.16).

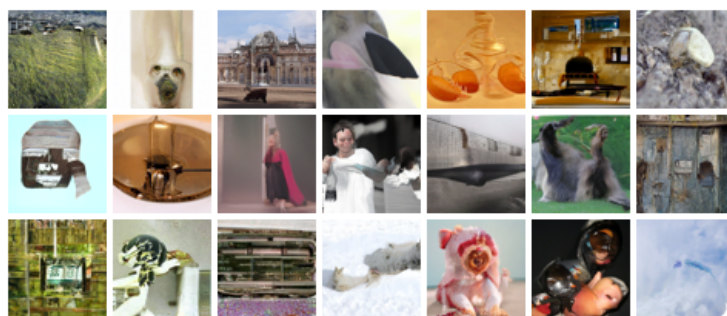


(b) Model obtained through LCSC (FID: 3.18).

Fig. 9: Generated images from a DM trained on CIFAR10 over 800K iterations.

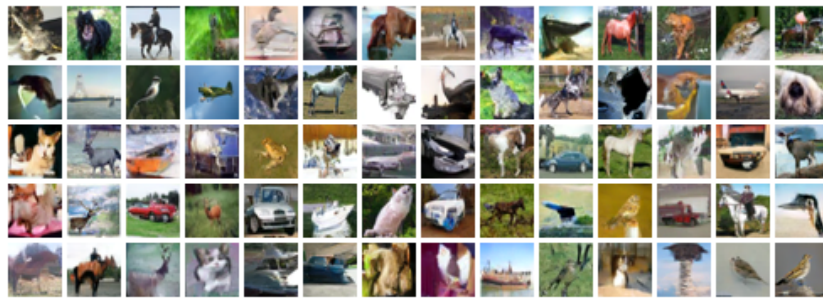


(a) EMA model (FID: 19.8).

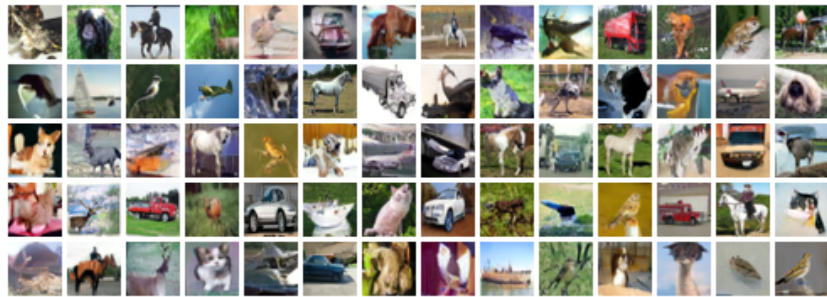


(b) Model obtained through LCSC (FID: 15.3).

Fig. 10: Generated images from a DM trained on ImageNet-64 over 500K iterations.



(a) EMA model (FID: 3.66).

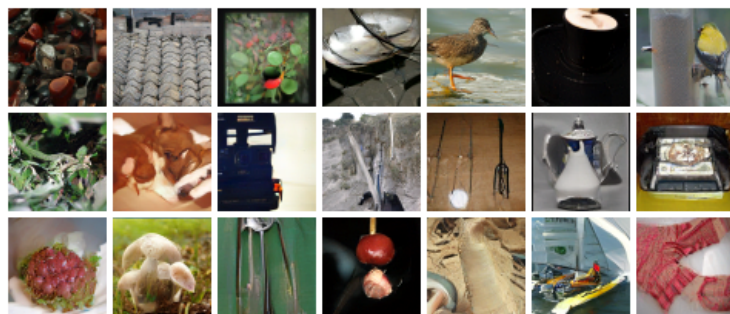


(b) Model obtained through LCSC (FID: 2.42).

Fig. 11: Generated images from a CD model trained on CIFAR10 for 800K iterations.

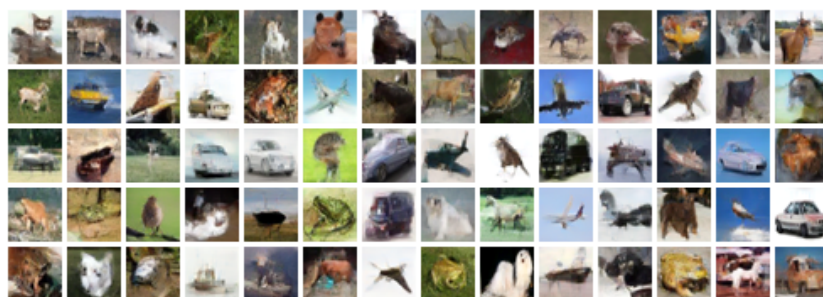


(a) EMA model (FID: 7.30).

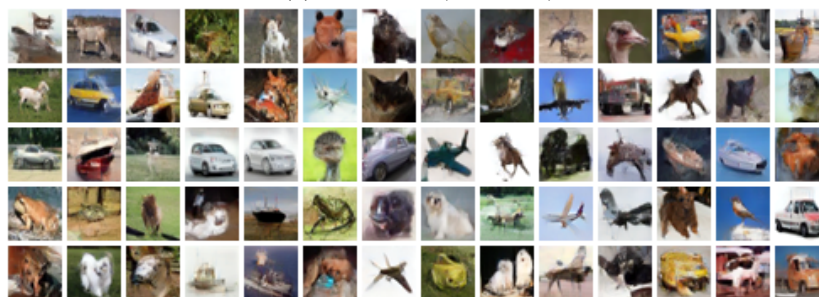


(b) Model obtained through LCSC (FID: 5.54).

Fig. 12: Images from a CD model trained on ImageNet-64 for 600K iterations.

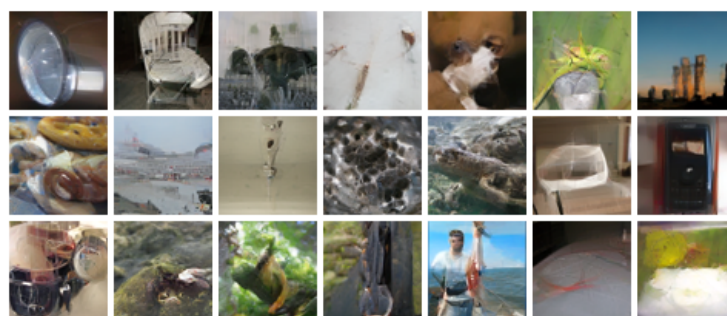


(a) EMA model (FID: 12.08).

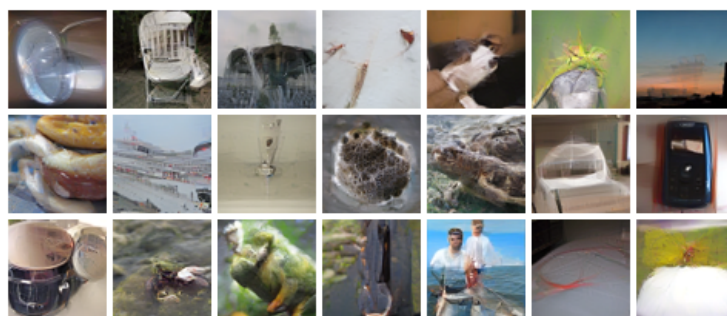


(b) Model obtained through LCSC (FID: 8.60).

Fig. 13: Generated images from a CT model trained on CIFAR10 for 400K iterations.



(a) EMA model (FID: 16.6).



(b) Model obtained through LCSC (FID: 12.1).

Fig. 14: Images from a CT model trained on ImageNet-64 for 600K iterations.